RESEARCH ARTICLE

ADVANCED
ELECTRONIC
MATERIALS
Open Access

www.advelectronicmat.de

Check for updates

Conjugated Polyimidazole Nanoparticles as Biodegradable Electrode Materials for Organic Batteries

Philipp A. Schuster, Matthias Uhl, Ann-Kathrin Kissmann, Felicitas Jansen, Tanja Geng, Maximilian U. Ceblin, Sarah Spiewok, Frank Rosenau, Timo Jacob, and Alexander J. C. Kuehne*

Conjugated polymers are promising active materials for batteries. Batteries not only need to have high energy density but should also combine safe handling with recyclability or biodegradability after reaching their end-of-life. Here, π-conjugated polyimidazole particles are developed, which are prepared using atom economic direct arylation adapted to a dispersion polymerization protocol. The synthesis yields polyimidazole nanoparticles of tunable size and narrow dispersity. In addition, the degree of crosslinking of the polymer particles can be controlled. It is demonstrated that the polyimidazole nanoparticles can be processed together with carbon black and biodegradable carboxymethyl cellulose binder as an active material for organic battery electrodes. Electrochemical characterization shows that a higher degree of crosslinking significantly improves the electrochemical performance and leads to clearer oxidation and reduction signals of the polymer. Polyimidazole as part of the composite electrode shows complete degradation by exposure to composting bacteria over the course of 72 h.

P. A. Schuster, F. Jansen, S. Spiewok, A. J. C. Kuehne
Institute of Organic and Macromolecular Chemistry
Ulm University
Albert-Einstein-Allee 11, 89081 Ulm, Germany
E-mail: alexander.kuehne@uni-ulm.de
M. Uhl, T. Geng, M. U. Ceblin, T. Jacob
Institute of Electrochemistry
Ulm University
Albert-Einstein-Allee 47, 89081 Ulm, Germany
A.-K. Kissmann, F. Rosenau
Institute of Pharmaceutical Biotechnology
Ulm University
Albert-Einstein-Allee 11, 89081 Ulm, Germany
T. Jacob
Helmholtz-Institute Ulm (HIU)
Helmholtzstr 11, 89081 Ulm, Germany
T. Jacob
Karlsruhe Institute of Technology (KIT)
P.O. Box 3640, 76021 Karlsruhe, Germany

1. Introduction

Batteries represent indispensable energy storage devices that greatly impact and aid our everyday lives. Especially due to the global shift from burning fossil fuels to sustainable energy sources, the demand for new types of batteries is increasing. Modern batteries require high energy densities and safe handling combined with recyclability or biodegradability after reaching their end-of-life.[1] Whereas organic batteries of today only represent a niche technology, they have the potential to overcome the lithium paradigm that currently applies to lightweight batteries.[2,3] To reduce our carbon footprint, avoid critical raw materials, and improve performance beyond the current state-of-the-art, new environmentally compatible materials need to be developed to produce the batteries of the future.[1] Organic polymers hold promise as active materials in batteries, which could fulfill these demands.

In particular, conjugated polymers are promising materials for polymer-based batteries and have been tested and applied for battery applications since the early 1980s.[4,5] The mechanical properties of conjugated polymers would allow the battery to be flexible and therefore to be integrated into completely new application environments. However, such organic polymer electrode materials are currently based on polyaniline, polypyrrole, polythiophene, polyphenylenes, polyanthraquinones, and polycarbazoles, none of which building blocks are available from natural resources or qualify for biodegradation (see Figure S1, Supporting Information). By contrast, there are biobased or bioinspired polymers that are explored as active materials for batteries, for example, polydopamine derivatives[6,7] or redox-active polypeptides.[8] Another biobased and bioinspired building block is the nitrogen-rich homolog of polypyrrole, namely polyimidazole, which features a five-membered ring with two nitrogen atoms. Imidazoles occur naturally for example in histidine, biotin, and imidazole alkaloids.[9,10] Therefore, nature has developed pathways for degrading such molecular motifs. Imidazole is degradable by reactive oxygen species, which occur in macrophages[11,12] or in composting bacteria.[13,14] On the one hand, polyimidazole has the potential to be compostable and biodegradable into amide and amino acid fragments.[11,15]

**ADVANCED
SCIENCE NEWS**

www.advancedsciencenews.com

**ADVANCED
ELECTRONIC
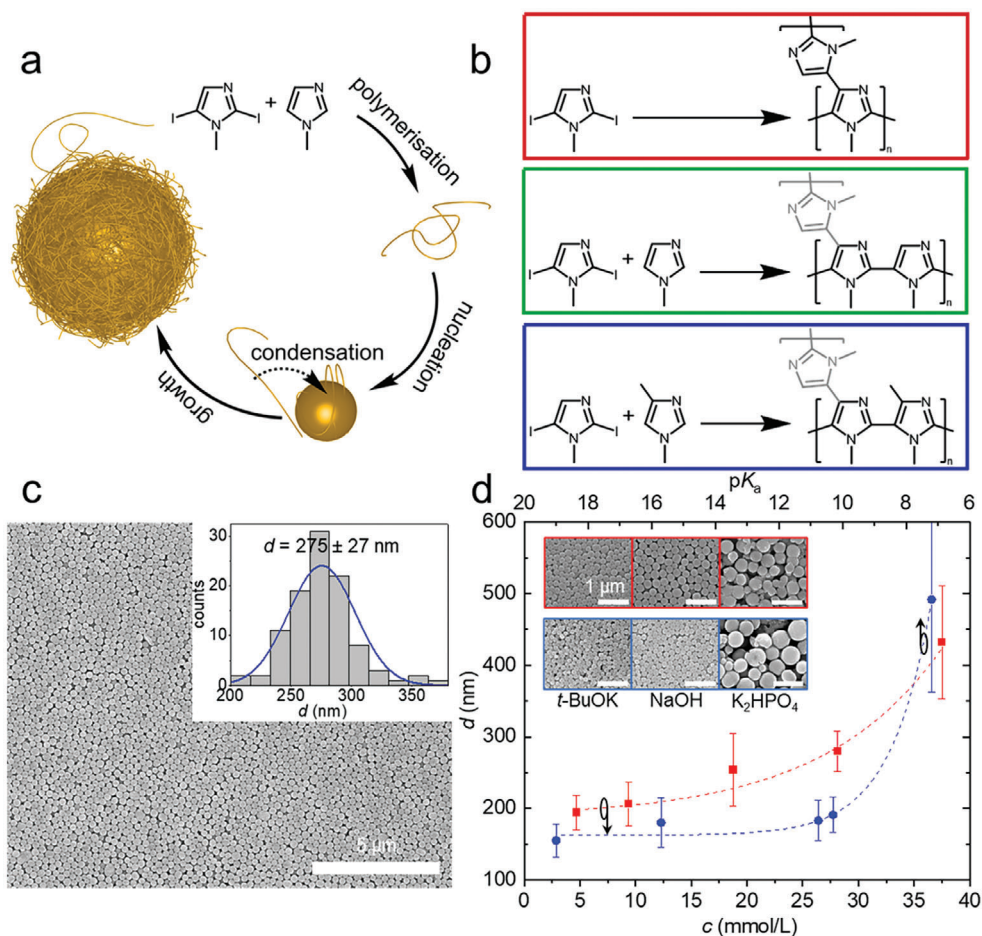MATERIALS**
Open Access

www.advelectronicmat.de

Figure 1. a) Schematic illustration of the dispersion polymerization of methylimidazole to particles. b) Synthesis scheme to produce polymers with different degrees of crosslinking. Polymers with (red) high, (green) medium, and (blue) low crosslink density. Reaction conditions are given in the materials and methods section. c) SEM images of the purified particles after 24 h reaction time. The inset shows a histogram of the particle diameters ($c = 28$ mmol L^{-1}, p$K_a = 10.7$). d) (Red) Particle size plotted against monomer concentration c and (blue) particle size versus pK_a of the base used. SEM image from left to right in blue the bases t-BuOK, NaOH, and K$_2$HPO$_4$, and in red the monomer concentrations 4.7, 28, and 37 mmol L^{-1}.

On the other hand, functional imidazole monomers are available from natural resources (such as glucose and other carbohydrates) through Radziszewski/Weidenhagen[16] or Windaus/Knoop syntheses.[17,18] Studies suggest that polyimidazoles could be oxidized as well as reduced rendering these materials interesting for application in symmetric organic batteries.[19] For example, an imidazole derivative, namely benzo diimidazole-dione shows excellent electrochemical properties in lithium-ion batteries.[20] However, there are currently neither studies that have characterized polyimidazoles in view of their performance as active materials in batteries, nor have polyimidazoles been explored as compostable electronic polymers that degrade in the presence of composting bacteria.

Here, we synthesize nanoparticles composed of imidazole homopolymers with tunable crosslink density and variable diameter. We evaluate the potential of imidazole nanoparticles as active materials in organic batteries and we establish biodegradability using bacteria that occur in soil and are typical for oxidative composting of organic matter.

2. Results and Discussion

2.1. Polymer Particles Synthesis

Instead of grinding or ball-milling a previously synthesized and precipitated active polymer material, which represents the typical preparation technique for the active material in organic batteries, we produce our active polyimidazole material as a dispersion of monodisperse nanoparticles (see **Figure 1a,c**). In short, we perform a direct arylation polymerization (DAP) between iodinated imidazole and the available C—H groups of respective imidazole co-monomers in a dispersion polymerization setup. The polymerization is conducted in 1-propanol, in which the monomers are soluble, as well as the palladium catalyst with adamantyl phosphine oxide ligands, and a base. Moreover, poly(vinylpyrrolidone-co-vinyl acetate) (PVPVA) and Triton X-45 are added to prevent aggregation and provide colloidal stability to the synthesized particles. Since 1-propanol is a solvent for the monomers but a non-solvent for the polymer, particles nucleate and grow during polymerization (see

ADVANCED
SCIENCE NEWS

www.advancedsciencenews.com

**ADVANCED
ELECTRONIC
MATERIALS**

www.advelectronicmat.de

Figure 1a).[21] In the absence of stabilizers, the polymer will precipitate in an uncontrolled fashion during synthesis, forming large aggregates that sediment (see Figure S2, Supporting Information). We perform dispersion polymerization using pure 2,5-diiodo-1-methyl-imidazole, where self-coupling between the iodo-groups and the C—H group in 4-position delivers polymer particles of high crosslink density (see Figure 1b, red). Coupling of 2,5-diiodo-1-methyl-imidazole with 1-methyl-imidazole results in medium crosslink density (see Figure 1b, green) and 1,4-dimethyl-imidazole, where the 4-position is protected by a methyl group and cannot participate in crosslinking, delivers low degrees of crosslinking (Figure 1b, blue). The advantage of crosslinked polymer particles is in their insolubility in the electrolyte even in the charged state. The particle diameter d increases with rising monomer concentration (see red curve and insets in Figure 1d). Surprisingly, the strength of the employed base also has an effect on the particle diameter, with stronger bases like potassium *tert*-butoxide (*t*-BuOK) delivering smaller d and weaker bases such as sodium hydroxide (NaOH) and dipotassium phosphate (K_2HPO_4) delivering larger d (see blue curve and insets in Figure 1d). Apparently, stronger bases lead to faster polymerization kinetics and therefore faster phase inversion, meaning more nuclei are being formed and an overall greater number of particles is growing. This leads to more but smaller particles at complete conversion. Here, all particle syntheses are carried out under argon-inert gas conditions. If the reaction mixture is not degassed and all other reaction conditions remain the same, the particle diameters become smaller by 15–20%, indicating slight deactivation of the catalyst.[21,22]

2.2. Electrochemical Characterization

To test the applicability of polyimidazole particles as redox-active battery electrodes, we investigate their electrochemical behavior using cyclic voltammetry (CV) in a Swagelok-type T-shaped 3-electrode cell setup with 1-butyl-1-methylpyrrolidinium bis(trifluormethylsulfonyl)imide ($Pyr_{14}TFSI$) in propylene carbonate as the electrolyte. $Pyr_{14}TFSI$ has a low viscosity of 3.7 mPa s and has proven suitable as an electrolyte for polymer electrodes.[23,24] The large size of the TFSI anion is advantageous, due to its small solvation shell.[25] We add Super P conductive carbon and carboxymethyl cellulose (CMC) as a biodegradable binder[26,27] to the polyimidazole particles. The ratio of Super P to polyimidazole particles is 6:3.5 by weight. The amount of binder is 5 wt%. We add the components to water (0.055 μS) to obtain a viscous slurry after homogenization using an ultra turrax. The slurry is then doctor-blade-coated onto aluminum foil (as a charge collector) and dried at room temperature in the air. The thickness is adjusted by tuning the gap of the doctor blade between 30 and 100 μm. Cross-sections recorded by scanning electron microscopy (SEM) corroborate that the polyimidazole particles and Super P particles are well mixed and show no obvious separation or sedimentation during drying (see Figure S3, Supporting Information). The specific surface area determined by gas adsorption, following Brunauer–Emmett–Teller (BET) theory, is 40.3 $m^2 g^{-1}$ for the composite electrode. For comparison the pure carbon black with binder has a BET surface of 60.7 $m^2 g^{-1}$, indicating that the polyimidazole particles have a

small surface area and are not porous. A previous study found irreversible electrochemical oxidation of imidazole-based polymers at 1.2 V (vs Ag) with a doping level (charges per monomer unit) of 0.3, which would result in a theoretical specific capacity of 112 mAh g^{-1}.[19] Our electrochemical characterization confirms this irreversible electrochemical degradation as soon as the stability window of polyimidazole is exceeded (see Figure S4, Supporting Information). We therefore limit the oxidation potential here to 1 V and observe at least partial reversibility. For our polyimidazole nanoparticles, oxidation takes place between 0.6 and 0.8 V and the respective reduction between 0.2 and 0.4 V (vs Ag), depending on the electrode composition (see **Figure 2**). The observed capacity is low compared to the previously reported values.[19] However, as reversibility is a mandatory requirement for battery application, further oxidation is not appropriate. It should also be mentioned that the partial oxidation is absent when using imidazole monomers. Therefore, the extended π-system seems to be a required precondition for the quasi-reversible uptake of electrons. To optimize the reversibility and the capacity of our polyimidazole active material, we tune the crosslink density, the particle diameter, the ratio of active material to conducting carbon filler, and the overall thickness of the electrode, expressed as mass loading (see Figure 2).

A higher degree of crosslinking clearly improves the electrochemical processes, leading to more distinct oxidation and reduction signals (see Figure 2a). The reason for this improvement could be the structural arrangement of the monomer as part of the conjugated polymer network. An increased degree of crosslinking will lead to a less delocalized π-conjugated system and therefore more discrete electrochemical signals. In addition, highly crosslinked polymers eliminate the problem of solubility of the organic active material in conventional electrolytes, which occurs with small organic molecules and leads to a rapid decrease in capacity.[28] We carry on with the medium crosslink density and synthesize particles of 210 ± 40 (small), 460 ± 60 (medium), and 510 ± 40 nm (large) in diameter. Electrochemical characterization by cyclic voltammetry delivers no clear size–property relationship (see Figure 2b). This is surprising, since for other polymers such as poly(2,2,6,6-tetramethyl-4-piperinidyl-*N*-oxyl methacrylate) such relationships between particle size, peak potential, and current have been reported.[23] Here, other effects, such as surface roughness, as well as gradients in crosslink density from the inside out of larger or smaller particles, may play a role.

Typically, the loading of active material has a strong impact on the capacity of the electrode. However, depending on the conductivity of the redox-active material a conducting carbon filler needs to be added. Here, we continue with crosslinked particles of $d = 450 \pm 50$ nm and vary the conductive Super P filler content from 30 to 80 wt%. At 80 wt% filler, we clearly observe much greater specific capacity with respect to the mass of polyimidazole than at 50 wt% and below, indicating only mediocre conductivity of our redox-active polyimidazole nanoparticles (see Figure 2c). However, the high capacity is the result of capacitive currents mainly caused by the conductive carbon additive, which almost completely masks the redox signals of the polyimidazole peaks. The lowest carbon content of 30 wt% is disadvantageous as the electrodes lack electrochemical stability. By contrast, in the case of 50 wt%, the peak currents for the polyimidazole
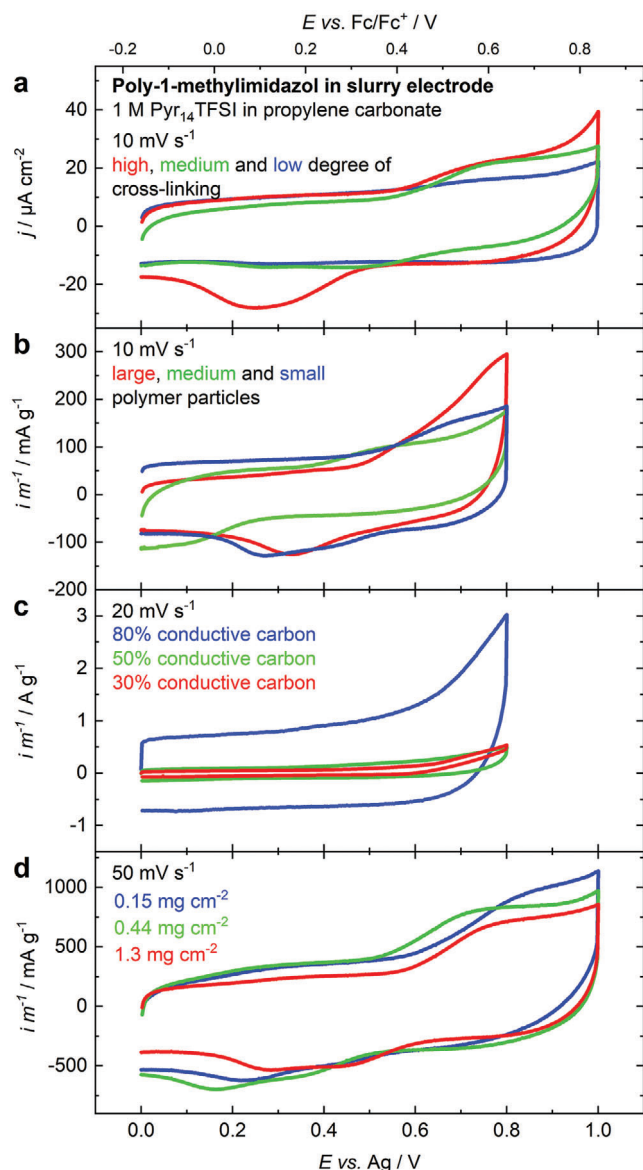
**ADVANCED
SCIENCE NEWS**

www.advancedsciencenews.com

**ADVANCED
ELECTRONIC
MATERIALS**

www.advelectronicmat.de

Figure 2. Influence of a) the degree of cross-linking, b) the particle size, c) the amount of carbon in the electrode slurry, and d) the mass loading on the electrochemical activity in CV of polymer electrodes based on polyimidazole. The individual scan rates and the modified parameters are given in the respective graphs. Potentials were measured using Ag wire as a reference electrode (bottom axis) and additionally referenced against ferrocene (top axis).

Figure 3. a) Specific charge (green) and discharge (orange) capacities of a slurry-based polyimidazole electrode in 1 M Pyr_{14}TFSI in propylene carbonate galvanostatically cycled with a rate of 10 C with respect to the experimentally determined capacity. The Coulombic efficiency of each cycle is shown in blue. b) Potential profiles of the 1st (blue), 5th (cyan), 10th (green), 20th (orange), and 100th (red) galvanostatic charging (dotted lines) and discharging (solid lines) of the measurement shown in (a).

even increase by cycling. As a result, we consider the optimum amount of conductive carbon to active material to be around 50 wt%. Continuing with this ratio of added Super P, we see no substantial influence of the electrode thickness on the aluminium collector electrode—or the mass loading of the organic electrode composite—on the capacity (see Figure 2d). An increase of the mass loading by a factor of nine only reduces the specific currents slightly (see Figure 2d). Therefore, we conclude that the electronic and ionic conductivity of the composite electrodes is
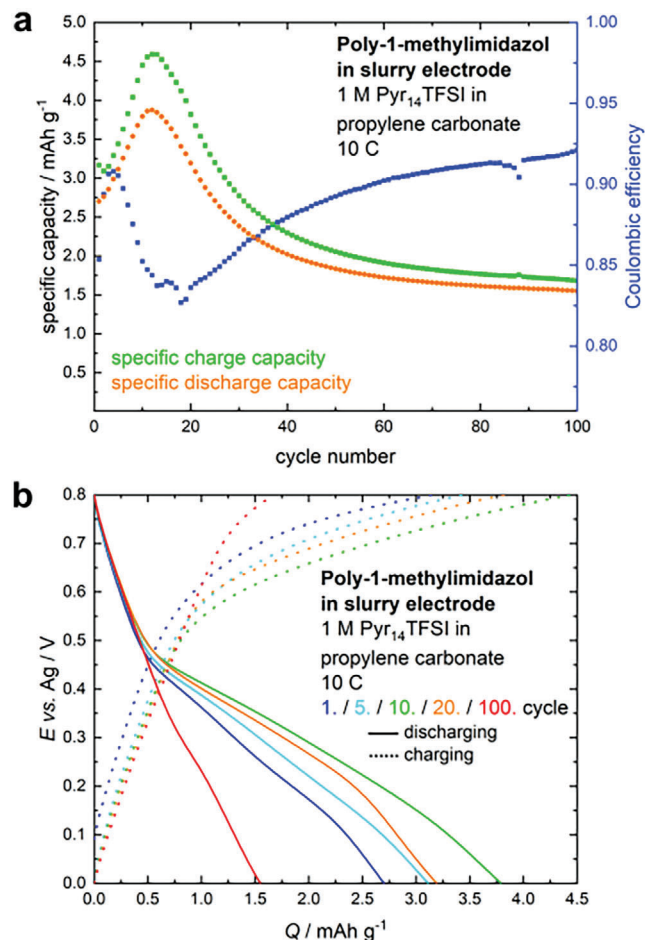
good and that the entire electrode contributes to the observed capacity.

The electrode performance improves during ongoing cycling over the course of 40 cycles, as can be seen in Figure S5, Supporting Information. The decomposition currents at the positive end of the potential stability window are decreasing, whereas the peak currents for the polyimidazole oxidation increase. In galvanostatic charge–discharge measurements with a rate of 10 C with respect to the experimentally determined capacity, a maximum capacity of 4.7 mAh g^{-1} is reached after initial conditioning, during which the electrode most probably gets soaked completely with electrolyte. Subsequently, the capacity is slowly fading with Coulombic efficiencies of 82–92% (see **Figure 3a**). These chronopotentiometric measurements are in agreement with the cyclic voltammetry in Figure S5, Supporting Information. During the first galvanostatic charging cycle, the polyimidazole oxidation is directly followed by initial decomposition currents, leading to a relevant amount of irreversible oxidation, as shown in

**ADVANCED
SCIENCE NEWS**

www.advancedsciencenews.com

**ADVANCED
ELECTRONIC
MATERIALS**

www.advelectronicmat.de

Figure 3b. During the first discharging cycle, the slope of the potential profile is less steep when the reduction potential is reached. As expected for conjugated polymers, no distinct potential plateaus are observed, since the oxidation and reduction potentials are dependent on the oxidation of the polymer with a distribution of possible states. With ongoing cycling, more charge is transferred at the potentials of the quasi-reversible oxidation of polyimidazole. After having passed the maximum capacity (cycle 13 in Figure 3a), the potential of the oxidative process is again increasing, resulting in an overall lower capacity and indicating degradation of the polyimidazole and passivation of the electrode. In the 100th cycle, currents attributed to Faraday processes are almost absent. The remaining capacitive currents are mainly caused by the conductive carbon in the slurry electrode. This is supported by electrochemical impedance spectroscopy indicating more capacitive behavior at low frequencies, while a clear semi-circle, which could be fitted with a simplified Randles circuit, can be observed in the high-frequency region of the Nyquist plot (see Figure S6, Supporting Information). During galvanostatic cycling, the cell resistance increases from 6.2 to 6.5 Ω and the charge-transfer resistance from 1.2 to 1.5 Ω, indicating slight passivation of the electrode.

2.3. Biodegradation Results

Conjugated polymer particles with imidazole co-monomers are known to degrade in the presence of reactive oxygen species. The imidazole unit can be cleaved oxidatively, leading to small molecular and non-toxic degradation products.[12] We perform degradation of our particles in solution of 30% H_2O_2 in water, and we record the diameter d via dynamic light scattering (DLS) over time. We observe a continuous decrease in d from $\approx$350 nm to fully degraded particles over the course of 8 h (see Figure S7, Supporting Information). The decrease in d is accompanied by an increase in the dispersity of the particle diameter, indicating that the particles do not degrade homogeneously from the outside in. More likely, the crosslinked particles will break up into smaller fragments that continue degrading—this model is in line with the accelerated degradation kinetics observed after $t = 210$ min, which is when the dispersity shoots up. When we analyze the isolated degradation products by chemical ionization (CI) mass-spectrometry (MS), we observe a main degradation product at $m/z = 129.1$, and a series of smaller fragmentation products. To make sure that this main degradation product is not a fragment produced during CI, we also perform MS with much gentler electrospray ionization (ESI-MS). Here we observe the same peak with $m/z = 129.102$ as well as another signal at $m/z = 174.160$, masses which correspond to the ring-opened degradation product of two adjacent imidazoles $C_6H_{13}N_2O^+$ and $C_8H_{20}N_3O^+$ (see Figure S8, Supporting Information). The latter signal is not apparent in CI-MS as it might be subject to fragmentation by the harsher chemical ionization. In combination, CI-MS and ESI-MS corroborate that the polyimidazole nanoparticles decompose in the presence of reactive oxygen into small molecular degradation products.

To investigate whether our electrodes manufactured as composites of polyimidazole particles with Super P and CMC will degrade in the presence of composting bacteria, we immerse the electrodes in a bacterial medium. However, naturally, the medium is aqueous and therefore dissolves the CMC binder, complicating the degradation study. Therefore, we first check the degradation of the imidazole polymer alone. We synthesize linear polyimidazole using Yamamoto coupling[21] ($M_n = 5100$ Da, $Đ = 1.1$) and dissolve the linear polymer in N-methyl-2-pyrrolidon to produce thin films on glass substrates by spin coating at a thickness of 0.3 µm.

The obtained polyimidazole films on glass are placed in bacterial media (lysogeny broth) containing bacteria that can be found in soil, manure, and compost, namely *Escherichia coli*,[29] the well-established biotechnological host strain *Pseudomonas putida* KT2440,[30-32] and the facultative pathogenic soil bacterium *Pseudomonas aeruginosa* (strains PAO1 and PA14),[33-37] which are known as producers of an impressive arsenal of extracellular (meaning secreted) enzymes and reactive oxygen species. After about 5 h at a temperature of 37 °C, holes become visible in the films colonized with the two *P. aeruginosa* strains, and after 24 h large parts of the film have been degraded completely (see Figure S9, Supporting Information). By contrast, *E. coli* requires 24 h to induce holes in the polyimidazole films and *P. putida* does not induce observable degradation of the film over the course of the 24 h experiment (see Figure S8, Supporting Information). The fastest degradation is observed for *P. aeruginosa* PAO1 (see **Figure 4**a–c). To investigate whether our crosslinked particles will also be degraded by *P. aeruginosa* PAO1, we mix the particles with a poly(vinylidene fluoride) (PVDF) binder that is insoluble in the bacterial medium. We compare the composites of particles with CMC binder to the PVDF-based composites by investigating the cross-section of the composite films by SEM. We find that the morphology of the films appears to be almost identical, with the polyimidazole particles being finely dispersed in the matrix of the binder (see Figure S3, Supporting Information). After exposure to the bacterial medium with *P. aeruginosa* PAO1 for 72 h the brown film turns white, indicating the disappearance of the brown polyimidazole particles (PVDF is white) (see Figure 4e). Inspecting the film after degradation with SEM, we find that the surface of the composite electrode is covered with a biofilm and individual *P. aeruginosa* PAO1 bacteria (see Figure 4g). To see if any particles remain underneath the biofilm, we enzymatically degrade the biofilm and bacteria for 30 min (Benzonase Nuclease from Merck Millipore). The exposed electrode exhibits large voids and an almost gyroidal scaffold of the binder, indicating that the enclosed imidazole polymer particles have been degraded (see Figure 4h). To confirm that the enzymatic degradation only degrades the bacteria and not the polyimidazole particles, we mix particles with bacteria in dispersion and add the enzyme. By taking samples and SEM images, we observed no change in particle size over 30 min. By contrast, the bacteria disappear (see Figure S10, Supporting Information). This is a clear indication that *P. aeruginosa* PAO1 is able to degrade linear polyimidazole as well as crosslinked polyimidazole particles. Finally, we investigate electrodes composed of our polyimidazole particles, PVDF binder, and Super-P carbon, to investigate whether the polyimidazole active material could also be degraded by composting bacteria in a realistic electrode composite. Since the color of the electrode is dominated by the black carbon particles, we cannot observe a change in the film before and after exposure to *P. aeruginosa* PAO1 by eye (see Figure 4i). However, the SEM image of the
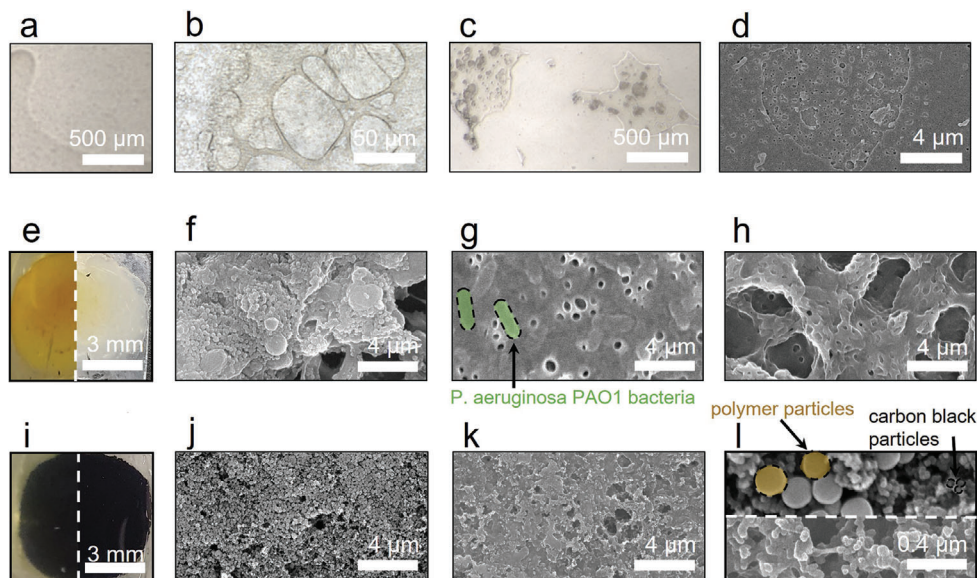
2300464 (5 of 7)

**ADVANCED
SCIENCE NEWS**

www.advancedsciencenews.com

**ADVANCED
ELECTRONIC
MATERIALS**

www.advelectronicmat.de

Figure 4. a) Linear poly(methylimidazole) prepared by Yamamoto coupling and spin-coated onto glass. b) Polyimidazole film (in (a)) treated with *Pseudomonas aeruginosa* PAO1 for 5 h at 37 °C. Large holes are visible under the light microscope. c) Same film as in (b) after 24 h. Large parts of the film are completely disintegrated. d) SEM image of the film and holes (in (b)) after 5 h. e) Polyimidazole particles mixed with PVDF binder and deposited on glass substrates by drop casting. Left shows the film in the beginning and the right after 72 h of bacterial treatment. f) SEM image of the Polyimidazole particles/PVDF film before treatment. g) same film as in (f) after 72 h of bacterial treatment. The green ovals highlight two of the bacteria present in the biofilm on the surface. h) SEM image shows the same film as in (g) after 30 min of treatment with the nuclease enzyme that degrades bacteria and biofilm. The biofilm is degraded and only the PVDF scaffold remains. i) Polyimidazole particles were mixed with PVDF binder and carbon black as for the electrochemical measurements and deposited on glass by drop casting. Left shows the film at the beginning and the right after 72 h of bacterial treatment. j) SEM image of the film in (i) before treatment, and k) after 72 h of bacterial treatment. l) Above shows the small carbon black and the much larger polyimidazole particles, before bacterial treatment. Below is the film after 72 h of incubation with the bacteria. The polyimidazole particles are degraded and the carbon black particles remain with the binder.

composite electrode allows clear differentiation of the small Super P carbon particles and the larger polyimidazole particles, held together by the PVDF binder (see Figure 4j,l (top)). After exposure to composting bacteria, we see that the electrode is coated by a biofilm and the larger polyimidazole particles are absent (see Figure 4k,l (bottom)). In combination, our study clearly corroborates that *P. aeruginosa* PAO1 as a model for composting bacteria can degrade redox-active polyimidazole particles from a functioning polymer battery electrode.

3. Conclusions

This work presents a starting point for biodegradable organic battery electrodes. Polyimidazole, here used as a redox-active battery material, exhibits only semi-reversible oxidation and reduction. Even though the capacity of this process is rather low compared to the theoretical value, we could investigate that crosslinking helps to increase the specific current of the redox process. Furthermore, polyimidazole shows full degradation by composting bacteria over the course of 72 h. Due to the very desirable biodegradability but rather low specific capacities, we propose that in the future imidazole could be combined with highly redox-active monomers in co-polymers for battery electrodes. With this, the capacity of the electrodes would be enhanced by mainly using the co-monomer for charge storage, while maintaining biodegradability through the imidazole units. Together with CMC as a water-soluble and degradable binder, the entire electrode will be compostable and

biocompatible. In view of the increasing demand for small-scale and printable energy storage devices, to power integrated sensors and wireless communication systems, our results represent an important contribution to the field of organic battery materials. When combined with environmentally friendly electrolytes—such as, for example, deep eutectic solvents[24]—our compostable electrodes could pave the way for completely biodegradable batteries.

Supporting Information

Supporting Information is available from the Wiley Online Library or from the author.

Conflict of Interest

The authors declare no conflict of interest.

Data Availability Statement

The data that support the findings of this study are available from the corresponding author upon reasonable request.

[1] M. D. Hager, B. Esser, X. Feng, W. Schuhmann, P. Theato, U. S. Schubert, *Adv. Mater.* **2020**, *32*, 2000587.

[2] B. Pan, J. Huang, Z. Feng, L. Zeng, M. He, L. Zhang, J. T. Vaughey, M. J. Bedzyk, P. Fenter, Z. Zhang, A. K. Burrell, C. Liao, *Adv. Energy Mater.* **2016**, *6*, 2.

[3] J. Bitenc, K. Pirnat, T. Bancic, M. Gaberscek, B. Genorio, A. Randon-Vitanova, R. Dominko, *ChemSusChem* **2015**, *8*, 4128.

[4] J. F. Mike, J. L. Lutkenhaus, *J. Polym. Sci., Part B: Polym. Phys.* **2013**, *51*, 468.

[5] S. Muench, A. Wild, C. Friebe, B. Häupler, T. Janoschka, U. S. Schubert, *Chem. Rev.* **2016**, *116*, 9438.

[6] K.-Y. Ju, Y. Lee, S. Lee, S. B. Park, J.-K. Lee, *Biomacromolecules* **2011**, *12*, 625.

[7] T. Sun, Z.-J. Li, H.-G. Wang, D. Bao, F.-L. Meng, X.-B. Zhang, *Angew. Chem.* **2016**, *128*, 10820.

[8] T. P. Nguyen, A. D. Easley, N. Kang, S. Khan, S.-M. Lim, Y. H. Rezenom, S. Wang, D. K. Tran, J. Fan, R. A. Letteri, X. He, L. Su, C.-H. Yu, J. L. Lutkenhaus, K. L. Wooley, *Nature* **2021**, *593*, 61.

[9] A. P. Santos, P. R. H. Moreno, in *Handbook of Natural Products*, (Eds.: K. G. Ramawat, J. M. Mérillon), Springer, Berlin **2013**, pp. 861–882.

[10] A. Vázquez-Salazar, A. Becerra, A. Lazcano, *PLoS One* **2018**, *13*, e0196349.

[11] E. Rorije, F. Germa, B. Philipp, B. Schink, D. B. Beimborn, *SAR QSAR Environ. Res.* **2002**, *13*, 199.

[12] T. Repenko, A. Rix, A. Nedilko, J. Rose, A. Hermann, R. Vinokur, S. Moli, R. Cao-Milàn, M. Mayer, G. Von Plessen, A. Fery, L. De Laporte, W. Lederle, D. N. Chigrin, A. J. C. Kuehne, *Adv. Funct. Mater.* **2018**, *28*, 1705607.

[13] M. Danon, I. H. Franke-Whittle, H. Insam, Y. Chen, Y. Hadar, *FEMS Microbiol. Ecol.* **2008**, *65*, 133.

[14] D. F. Berry, A. J. Francis, J. M. Bollag, *Microbiol. Rev.* **1987**, *51*, 43.

[15] B. Philipp, M. Hoff, F. Germa, B. Schink, D. Beimborn, V. Mersch-Sundermann, *Environ. Sci. Technol.* **2007**, *41*, 1390.

[16] R. Weidenhagen, R. Herrmann, *Chem. Ber.* **1935**, *68*, 1953.

[17] A. Bhatnagar, P. K. Sharma, N. Kumar, *Int. J. PharmTech Res.* **2011**, *3*, 268.

[18] K. Hofmann, in *Chemistry of Heterocyclic Compounds*, (Ed.: A. Weissberger), Interscience Publishers, Inc., New York **1953**, p. 421.

[19] T. Yamamoto, T. Uemura, A. Tanimoto, S. Sasaki, *Macromolecules* **2003**, *36*, 1047.

[20] L. Zheng, J. Ren, H. Ma, M. Yang, X. Yan, R. Li, Q. Zhao, J. Zhang, H. Fu, X. Pu, M. Hu, J. Yang, *J. Mater. Chem. A* **2022**, *11*, 108.

[21] F. Jansen, P. A. Schuster, M. Lamla, C. Trautwein, A. J. C. Kuehne, *Biomacromolecules* **2021**, *22*, 5065.

[22] L. Ackermann, S. Barfüsser, C. Kornhaass, A. R. Kapdi, *Org. Lett.* **2011**, *13*, 3082.

[23] S. Muench, P. Gerlach, R. Burges, M. Strumpf, S. Hoeppener, A. Wild, A. Lex-Balducci, A. Balducci, J. C. Brendel, U. S. Schubert, *ChemSusChem* **2021**, *14*, 449.

[24] M. Uhl, T. Geng, P. A. Schuster, B. W. Schick, M. Kruck, A. Fuoss, A. J. C. Kuehne, T. Jacob, *Angew. Chem., Int. Ed.* **2023**, *62*, e202214927.

[25] Y. Zhang, L. Zhao, Y. Liang, X. Wang, Y. Yao, *eScience* **2022**, *2*, 110.

[26] C. G. Van Ginkel, S. Gayton, *Environ. Toxicol. Chem.* **1996**, *15*, 270.

[27] J. S. Yaradoddi, N. R. Banapurmath, S. V. Ganachari, M. E. M. Soudagar, N. M. Mubarak, S. Hallad, S. Hugar, H. Fayaz, *Sci. Rep.* **2020**, *10*, 21960.

[28] K. S. Weeraratne, A. A. Alzharani, H. M. El-Kaderi, *ACS Appl. Mater. Interfaces* **2019**, *11*, 23520.

[29] U. Sonnenborn, *FEMS Microbiol. Lett.* **2016**, *363*, fnw212.

[30] K. E. Nelson, C. Weinel, I. T. Paulsen, R. J. Dodson, H. Hilbert, V. A. P. Martins Dos Santos, D. E. Fouts, S. R. Gill, M. Pop, M. Holmes, L. Brinkac, M. Beanan, R. T. Deboy, S. Daugherty, J. Kolonay, R. Madupu, W. Nelson, O. White, J. Peterson, H. Khouri, I. Hance, P. C. Lee, E. Holtzapple, D. Scanlan, K. Tran, A. Moazzez, T. Utterback, M. Rizzo, K. Lee, D. Kosack, et al., *Environ. Microbiol.* **2002**, *4*, 799.

[31] I. Bator, A. Wittgens, F. Rosenau, T. Tiso, L. M. Blank, *Front. Bioeng. Biotechnol.* **2020**, *7*, 480.

[32] A. Wittgens, B. Santiago-Schuebel, M. Henkel, T. Tiso, L. M. Blank, R. Hausmann, D. Hofmann, S. Wilhelm, K.-E. Jaeger, F. Rosenau, *Appl. Microbiol. Biotechnol.* **2018**, *102*, 1229.

[33] R. Hoge, A. Pelzer, F. Rosenau, S. Wilhelm, in *Current research, technology and education topics in applied microbiology and microbial biotechnology*, Vol.*2*, Formatex Research Center, Spain **2010**, p. 383.

[34] C. K. Stover, X. Q. Pham, A. L. Erwin, S. D. Mizoguchi, P. Warrener, M. J. Hickey, F. S. L. Brinkman, W. O. Hufnagle, D. J. Kowalik, M. Lagrou, R. L. Garber, L. Goltry, E. Tolentino, S. Westbrock-Wadman, Y. Yuan, L. L. Brody, S. N. Coulter, K. R. Folger, A. Kas, K. Larbig, R. Lim, K. Smith, D. Spencer, G. K.-S. Wong, Z. Wu, I. T. Paulsen, J. Reizer, M. H. Saier, R. E. W. Hancock, S. Lory, et al., *Nature* **2000**, *406*, 959.

[35] R. Hoge, M. Laschinski, K.-E. Jaeger, S. Wilhelm, F. Rosenau, *FEMS Microbiol. Lett.* **2011**, *316*, 23.

[36] S. Wilhelm, A. Gdynia, P. Tielen, F. Rosenau, K.-E. Jaeger, *J. Bacteriol.* **2007**, *189*, 6695.

[37] J. He, R. L. Baldini, E. Dé, M. Saucier, Q. Zhang, N. T. Liberati, D. Lee, J. Urbach, H. M. Goodman, L. G. Rahme, *Proc. Natl. Acad. Sci.* **2004**, *101*, 2530.